Experimental study on breakup of a single bubble in a stirred tank: Effect of gas density and liquid properties

Huahai Zhang, Yuelin Wang, Ali Sayyar, Tiefeng Wang*

Beijing Key Laboratory of Green Reaction Engineering and Technology

Department of Chemical Engineering, Tsinghua University, Beijing 100084, China

Correspondence author: Tiefeng Wang (E-mail: wangtf@tsinghua.edu.cn)

Abstract: Bubble breakup plays an important role in gas-liquid flows, but detailed studies are still scarce. In this work, the breakup behavior of a single bubble in a stirred tank was experimentally studied with a high-speed camera, focusing on the effect of gas density, liquid properties, agitation speed and mother bubble size. The bubble breakup time, breakup probability, breakup rate and daughter bubble size distribution were determined. The internal flow phenomenon inside a deformed bubble was studied in detail, which accounted for the effect of gas density or operating pressure. The results showed that with increasing gas density, agitation speed, mother bubble size and decreasing surface tension, the bubble breakup rate and probability of equal-size distribution significantly increased. With increasing liquid viscosity, the bubble breakup rate decreased especially in the high viscosity range. An M-shaped daughter bubble size distribution was observed, which was consistent with our previous bubble breakup model.

Keywords: Bubble breakup; Stirred tank; Gas density; Liquid properties; Internal flow

1. Introduction

The dispersion of bubbles in a continuous liquid flow exists in many industrial processes, such as chemical, petroleum, pharmaceutical and food industries. The bubble size distribution, which is a result of the balance between breakup and coalescence,[1,2] is a key parameter for the gas-liquid interfacial area and the momentum, mass and heat transfer rates.[3-6] The population balance model (PBM), which was firstly proposed by Hulburt and Katz[7], can be used to predict the bubble size distribution. The PBM equation for the gas-liquid bubbly flow is expressed by:[8,9]

$$
\underbrace{\frac{\partial n(v,t)}{\partial t}}_{\text{I}} + \underbrace{\nabla \cdot \left[\boldsymbol{u}_{\text{b}} n(v,t) \right]}_{\text{II}} = \underbrace{\frac{1}{2} \int_0^v n(v-v',t)n(v',t)c(v-v',v')dv'}_{\text{III}}
$$
$$
- \underbrace{\int_0^\infty n(v,t)n(v',t)c(v,v')dv'}_{\text{IV}} + \underbrace{\int_v^\infty \beta(v,v')b(v')n(v',t)dv'}_{\text{V}} - \underbrace{b(v)n(v,t)}_{\text{VI}}
$$

(1)

where the subscripts describe (I) time variation, (II) convection, (III) source resulted from coalescence, (IV) sink resulted from coalescence, (V) source resulted from breakup, and (VI) sink resulted from breakup. To solve Eq. (1), the breakup rate $b(v)$, coalescence rate $c(v)$ are necessary. Over three decades, many bubble breakup models have been developed, as reviewed by Liao and Lucas[10] and Solsvik et al.[11] However, reliable experimental data of bubble breakup are very scarce, therefore it is difficult to evaluate the accuracy of the bubble breakup models.

Four mechanisms of bubble breakup were reported in the literature: turbulent fluctuation and collision, viscous shear stress, shearing-off process, and interfacial instability.[10,11] In a fully developed turbulent flow, the dominant mechanism was the breakup due to collision by turbulent eddies. Therefore, most experiments on bubble

breakup in the literature were realized by creating turbulence and then breaking up the bubbles. According to the ways of producing turbulence, previous experiments on bubble breakup can be categorized as follows:

(1) Increasing the liquid velocity in a pipe[12-14] or a narrow gap of a homogenizer[15-17] and producing high-speed jet flow[18-23] to enhance turbulence. Although the turbulence was nearly homogeneous, the liquid flow rate was very large and the intensity of produced turbulence was relatively low. In addition, the apparatus was complex and the operating liquid was difficult to replace. Due to the high liquid velocity, the images of bubble deformation were very ambiguous and difficult to analyze.

(2) Creating mechanical agitation in a stirred vessel[24-31] to produce turbulence. The experimental operation was easy in a small stirred tank without liquid circulation. However, the flow was mostly inhomogeneous, therefore the situation changed from bubble primary deformation to final breakup. The bubbles broke up more frequently near the stirrer blade than in other zones. Furthermore, bubbles sometimes broke up due to cut by the blade.

(3) Creating turbulent pipe flow[32] or conical channel flow[33] by using a paddle in a liquid circulating reactor with baffles under the paddle to enhance turbulence. Compared to the liquid flow in a stirred tank, the turbulent pipe or conical channel flow was more homogeneous, but a liquid circulation was needed and the experimental apparatus was quite complex. In addition, the turbulent intensity was still low in this apparatus.

(4) Adding internals or obstacles to promote turbulence.[34,35] However, such kinds

of internals or obstacles had a significant effect on the experimental results, and the design of internals and obstacles was rather complicated.

Although extensive experimental studies were reported on bubble breakup, most of them were qualitative and focused on the breakup phenomena and mechanism. Very limited experimental data were reported on the bubble breakup time, breakup probability, daughter size distribution, and especially the breakup rate. Moreover, the quantitative influences of the operating conditions and the gas or liquid properties on bubble breakup were not clearly studied. However, such experimental data were highly required for validation of the bubble breakup model.

The present work aimed to study the bubble breakup in a stirred tank that was specially designed to produce homogeneous turbulence with a high intensity. The effect of gas density or pressure, liquid properties, agitation speed and mother bubble size on the bubble breakup behaviors, such as the breakup time, daughter size distribution, and breakup rate were systemtically investigated. Then, the measured bubble breakup rates and daughter size distributions were used to validate our previous bubble breakup model[36]. In addition, the phenomenon of internal flow[35] during bubble deformation and breakup process was clearly observed in our experiment, which was closely related to the effect of gas density or pressure on bubble breakup.

2. Experimental

2.1. Experimental setup

The schematic diagram of the experimental setup is shown in Fig. 1. The bubble breakup experiments were carried out in a cylindrical glass tank with four evenly

distributed plate baffles ($15 \times 3 \times 220$ mm). The tank was 220 mm in height, 200 mm in inner diameter, and 5 mm in wall thickness. The impeller structure was shown in Fig. 2. It had a diameter of 12 mm and contained four equispaced plate blades of 200 mm high, 25 mm wide and 2 mm thick. The distance between the impeller and tank bottom was 2 mm. One round plate of 31 mm in diameter was put on top of the impeller to prevent air from being sucked into the tank. The rotating speed of the impeller was varied from 480 to 640 rpm. A high-speed camera (Photron UX 50, 2000 fps, 1024×1280 pixel/cm^2) was used to record the whole bubble deformation process from entering the observation area until bubble breakup occurred or the bubble exited the region of interest. The bubbles were generated with the gas from gas cylinders (He, N_2, and SF_6) using a stainless steel tube of different diameters ($d_t = 1, 3, 4$ and 6 mm). A toroidal hat (13 mm I.D.) equipped at the end of the tube was used by Hasan[30] to assure that the bubbles would not be disturbed before releasing into the liquid, and this method was used in our experiments. The detailed size and arrangement of the experimental apparatus are shown in Fig. 2. Different gas and liquid were used, and their properties are listed in Table 1.
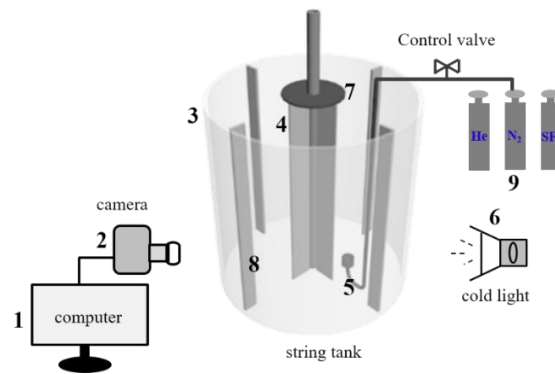

Figure 1. Experimental setup. 1-computer, 2-high-speed camera, 3-glass tank, 4-stirring impeller, 5-bubble generator, 6-cold light, 7-round plate, 8-baffles, 9- gas cylinder.
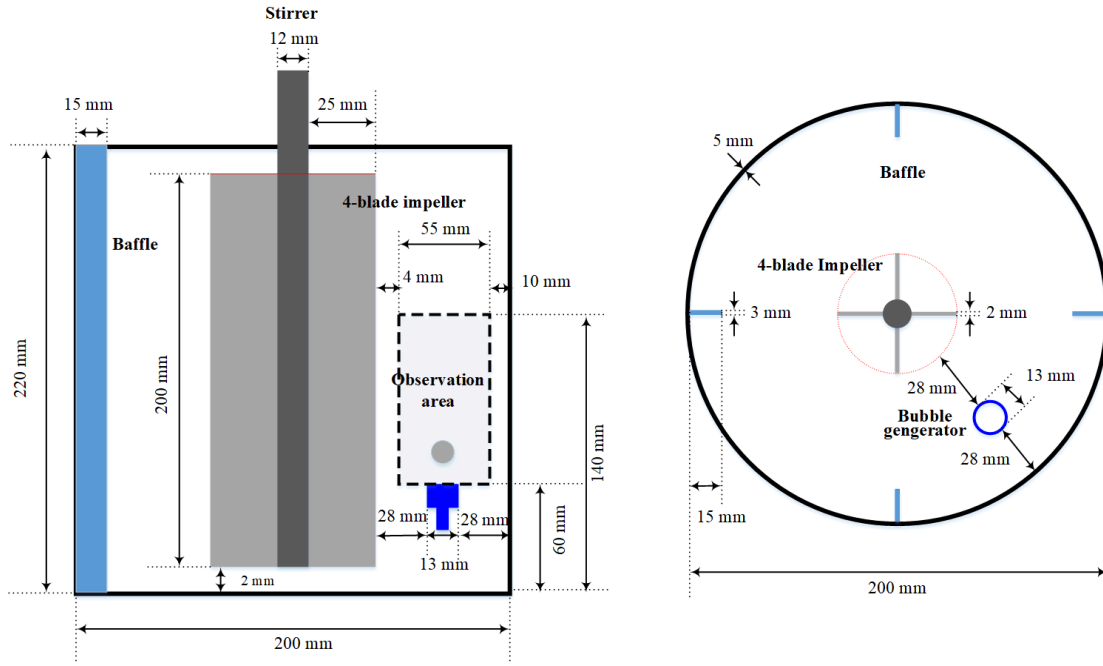
Figure 2. Front (left) and top (right) view of the tank.

Table 1. Properties of used gas and liquid.

	Gas/Liquid	ρ, kg/m^3	μ_l, mPa·s	σ_l, mN/m
Gas	He	0.16		
	N$_2$	1.18		
	SF$_6$	6.16		
Liquid	Water	1000	1.0	72.5
	95 wt% Ethanol	780	1.0	22.3
	54.9 wt% glycerol	1124	7.9	63.6
	76.6 wt% glycerol	1184	39.6	62.1

In each experiment, a single bubble was released at the bottom of the tank. The high speed camera with a minimum time interval of 0.5 ms was used to record the whole bubble deformation and breakup process, from which the bubble breakup time t_b, bubble breakup probability $P(d_b)$, and daughter bubble size distributions $\beta(f_v)$ were measured. When estimating the bubble breakup probability, ~200 bubble breakup events were analyzed. The bubble breakup rate $b(d_b)$ was calculated as follows:[19,37]

$$b(d_b) = \frac{1}{\text{breakup time}} \times \frac{\text{number of breakups of bubbles}}{\text{total number of bubbles}} = \frac{1}{t_b} P(d_b) \qquad (2)$$

2.2. Estimation of local turbulent dissipation rates

Five agitation speeds (n), including 480, 520, 560, 600 and 640 rpm, were used in the experiments to study the effect of turbulent dissipation rates on the bubble breakup. The local mean turbulent dissipation rates were determined from computational fluid dynamics (CFD) simulations with the Reynolds-averaged Navier-Stokes (RANS) two-fluid model and k-ε turbulence model, which had been used by many researchers for modeling stirred vessels.[31,38-42] In this work, the accuracy and reliability of the RANS k-ε model were validated by simulating the same stirred tank reported by Wu and Patterson[43] and comparing with their experimnetal data. A good agreement was obtained between the simulated mean tangential velocity, radial velocity and axial velocity profiles and experimental results at various radial positions, as shown in the Supporting Information (Figs. S1-S3). Fig. 3 shows the simulation domain and the structured Tet/Hybrid-grids drawn by Gambit. The stationary region (Fig. 3b) consisted of 1.2 million nodes, and the rotating region (Fig. 3c) had 0.9 million nodes. The maximum grid size for stationary and rotating region was 1.5 mm and 0.75 mm, respectively, and the minimum grid size in the interface between the two regions was 0.15 mm. The results of mesh independence test using three different grids, namely the coarse mesh (0.8 + 0.6), the chosen medium mesh (1.2 + 0.9), and the fine mesh (1.5 + 1.2), showed that the error of predicted mean turbulent dissipation rates was within 6%.
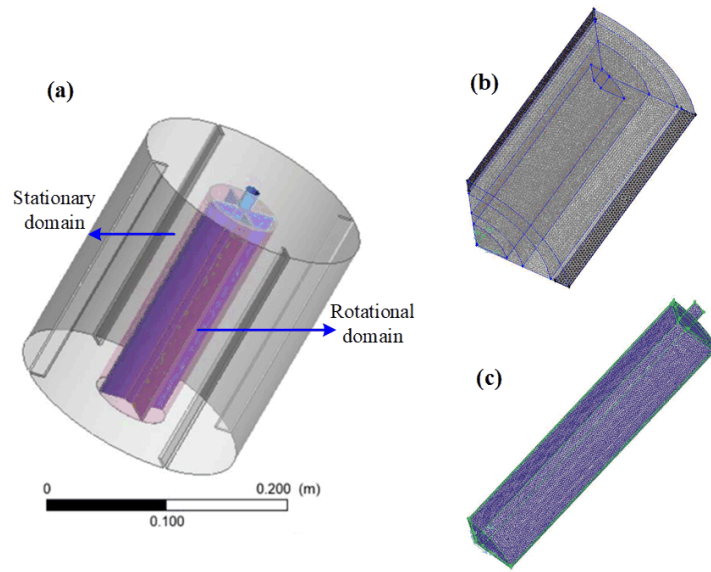
Figure 3. CFD simulation domains and meshes: (a) geometry for simulation, (b) grid details of the 1/4 stationary region, and (c) grid details of the 1/4 rotating region.

2.3. Measuring methods

2.3.1. Bubble breakup probability

The bubble breakup probability $P(d_b)$ was determined as the percentage of broken bubbles among the total bubbles. In each experimental process, no other bubbles existed in the stirred tank when observing the bubble deformation of one bubble. The case in which the bubble broke up before leaving the observation area was considered as a bubble breakup event. The data of more than 200 bubbles were collected for statistics to determine the bubble breakup probability.

2.3.2. Bubble breakup time

Due to the complexity of the bubble breakup behavior, the bubble breakup time has been determined very differently in the literature. Vejražka et al.[18] recorded the bubble breakup time starting from when the bubble entered the observing zone, ending when the bubble broke up or exited the zone. With this approach, the bubble breakup

time was overestimated because the bubble might not deform when arriving at the zone. Solsvik and Jakobsen[44] considered the bubble breakup time as the period between the beginning of bubble deformation and the final breakup. However, it was difficult to identify when the bubble began to deform. In this work, the situation when the surface of the bubble was markedly dented was determined as the starting moment. Fig. 4 shows a typical bubble breakup process, where the bubble breakup time from initial deformation to final breakup was ~18 ms. The mean bubble breakup time under a specific condition was determined based on more than 100 bubbles.
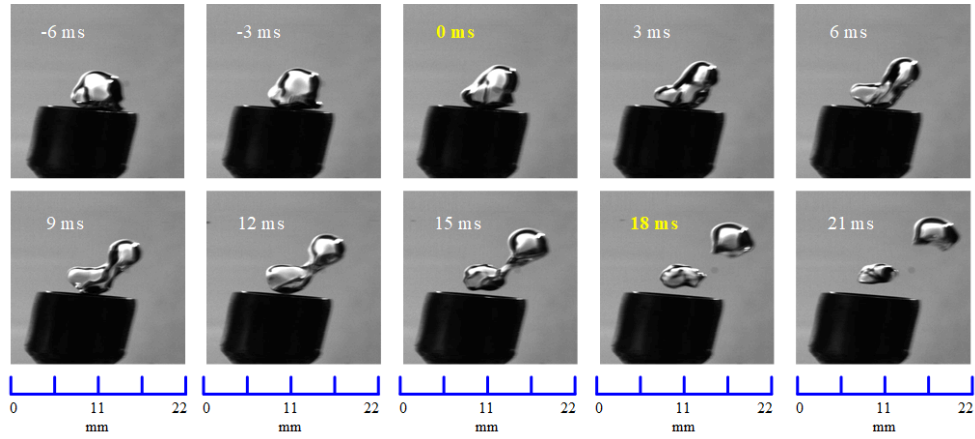

Figure 4. Breakup of a gas bubble into two fragments (water-N_2, n = 480 rpm, d_t = 4 mm).

2.3.3. Daughter bubble size distribution

For calculating the daughter bubble size distribution, the size of mother bubble was needed. For each condition, more than 100 images of the mother bubbles were obtained by the Photron Fastcam Viewer (PFV) image processing software. Fig. 5 shows the process of measuring the size of mother bubble. These mother bubbles, which were assumed to be ellipsoid, were identified through MATLAB grayscale recognition. The length of the long axis (2a) and short axis (2b) were determined, then the equivalent

diameter (d_e) was calculated as

$$d_e = \left[(2a)^2 \cdot 2b \right]^{1/3} \tag{3}$$

The daughter bubble size distribution was described by the bubble breakup ratio f_v as follows:

$$f_v = \frac{d_i^3}{(d_i^3 + d_j^3)} \tag{4}$$

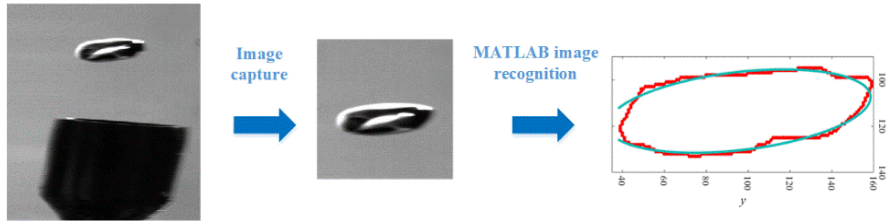where d_i and d_j were the diameter of two daughter bubbles.

Figure 5. Schematic diagram of image processing process.

3. Results and discussion

3.1. Turbulent energy dissipation rate

Three-dimensional transient simulations were carried out with the RANS k-ε model on Fluent 18.0 to determine the local mean turbulent energy dissipation rate in the observing area. The time interval was set at 0.001 s, and the total simulation time was 10 s. Fig. 6 shows the simulation results of turbulent dissipation rate under five agitation speeds. It can be found that the flow in the observation zone enclosed by the rectangle was nearly homogeneous, where the mean turbulent dissipation rate was determined as 0.67, 0.84, 1.02, 1.28 and 1.59 m^2/s^3 at the agitation speed of 480, 520, 560, 600 and 640 rpm, respectively.
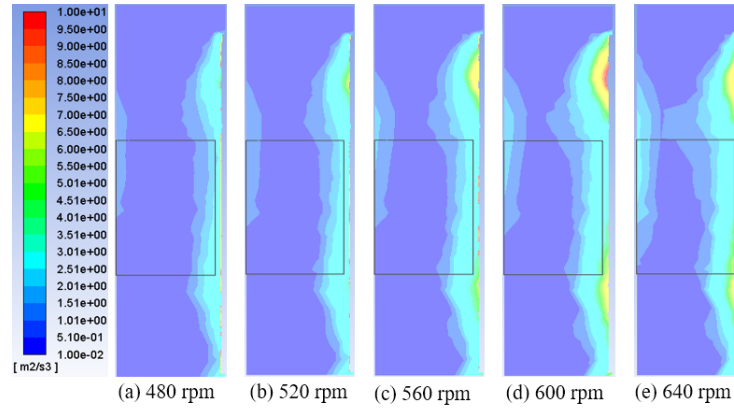
Figure 6. The simulated turbulent dissipation rates under different agitation speeds.

3.2. Bubble breakup rate

The bubble breakup time t_b and breakup probability $P(d_b)$ at different conditions are listed in Tables 2 and 3. The specific bubble breakup rate was calculated from t_b and $P(d_b)$ by Eq. (2). The effect of the mother bubble size on the bubble breakup was studied by using tubes of four different diameters to generate different sizes of mother bubbles. In the water-N_2 system, the mean diameter of the mother bubbles (d_b) generated by these four tubes was 2.4, 3.4, 4.2 and 7.9 mm. Meanwhile, to explore the effect of pressure or gas density on the bubble breakup, three kinds of gas, namely He, N_2 and SF_6, were used. Different liquids were chosen to study the effect of liquid properties.

Table 2. Effect of agitation speed on bubble breakup time t_b and breakup probability $P(d_b)$ in N_2-water system.

Agitation speed n (rpm)	Tube diameter d_t (mm)							
	1.0		3.0		4.0		6.0	
	$P(d_b)$ (%)	t_b (ms)	$P(d_b)$ (%)	t_b (ms)	$P(d_b)$ (%)	t_b (ms)	$P(d_b)$ (%)	t_b (ms)
480	10.5	18.4	26.5	20.4	47.0	24.9	61.9	26.1
520	15.0	15.0	28.0	17.9	48.0	19.3	66.5	20.8
560	18.0	14.1	32.5	16.0	50.0	16.4	67.5	16.7
600	23.0	13.1	37.0	14.3	53.0	14.5	70.0	14.7
640	30.5	11.2	43.5	13.5	62.0	13.8	82.0	12.9

Table 3. Effect of gas and liquid properties on bubble breakup time t_b and breakup probability $P(d_b)$ at an agitation speed of 480 rpm.

Liquids	Gas	Tube diameter d_t (mm)							
		1		3		4		6	
		$P(d_b)$	t_b	$P(d_b)$	t_b	$P(d_b)$	t_b	$P(d_b)$	t_b
		(%)	(ms)	(%)	(ms)	(%)	(ms)	(%)	(ms)
Ethanol	N_2	30.0	12.6	57.0	14.0	72.5	15.0	92.0	15.4
Water	N_2	10.5	18.4	26.5	20.4	47.0	24.9	61.9	26.1
Water	He	8.0	20.0	24.0	22.2	37.0	31.1	51.6	26.5
Water	SF_6	13.0	14.0	15.6	19.2	62.5	20.3	78.5	23.4
54.9% glycerol	N_2	6.0	19.0	32.0	21.3	44.0	23.8	57.0	26.5
76.6% glycerol	N_2	0.5	18.5	15.0	20.6	19.0	21.9	25.0	26.4
76.6% glycerol	SF_6	0.5	16.0	16.0	20.0	18.0	20.7	26.0	21.7

3.2.1. Effect of turbulent energy dissipation rate

The effect of the agitation speed on the bubble breakup probability and breakup time with different mother bubble sizes are shown in Fig. 7. It can be seen that the bubble breakup probability increased and the breakup time decreased with increasing agitation speed. When the agitation speed increased from 480 to 640 rpm, the mean turbulent energy dissipation rate increased from 0.67 to 1.59 m^2/s^3. The turbulent eddies with a higher turbulent energy dissipation rate contained more energy to collide with the mother bubbles and caused breakup, leading to higher breakup probability under high agitation speed. According to our previous breakup model[36,45], with increasing turbulent dissipation rate, the turbulent eddy velocity increased and therefore the time for shrinking of bubble neck decreased.

Figure 7 shows that with increasing mother bubble diameter, the bubble breakup probability significantly increased, which was in agreement with the experimental results in the literature.[12,25,44] The reason was that a larger bubble was less resistant to

the disruptive forces exerted by turbulent eddies. In addition, the probability of collision by turbulent eddies for a bubble increased with the bubble size. However, with increasing mother bubble size, the breakup time t_b first slightly increased and then remained nearly unchanged. Solsvik et al.[44] analyzed their measured bubble breakup time data and found that there was no general trend between the breakup time and the mother bubble size and stirring speed due to the lack of numerous experimental data. According to our previous model[36,45], with increasing mother bubble size, the time for shrinking of bubble neck and the bubble breakup time t_b would increase due to an increased length of bubble neck.
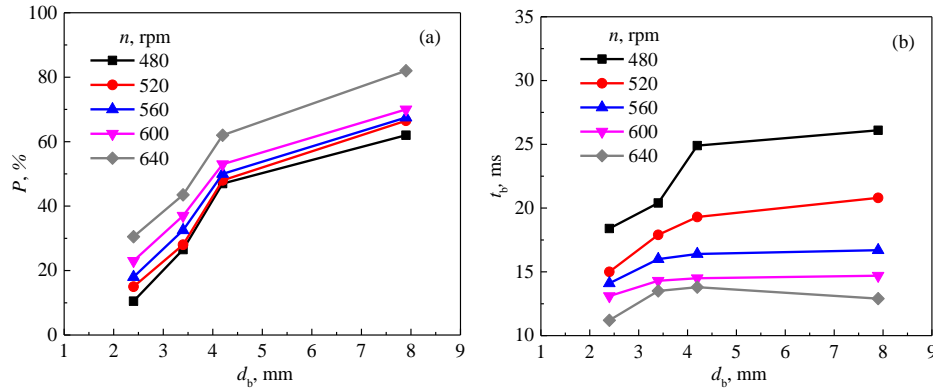
Figure 7. Effect of turbulent dissipation rates on (a) bubble breakup probability and (b) breakup time in a water-N_2 system.

Figure 8 shows the influence of the turbulent energy dissipation rate and mother bubble size on the bubble breakup rate. The error bars, determined by the standard deviation of the mean bubble diameter (σ_d) and mean bubble breakup rate (σ_b), were used to reflect the experimental uncertainty. The results showed that the breakup rate increased with increasing mother bubble size, which was consistent with the trends reported in other experimental results[12,18,19] and bubble breakup models[1,45-48]. The

bubble breakup rates predicted by our improved model[36] were in a satisfactory agreement with the experimental data. The deviation was likely attributed to the assumption of spherical bubbles used in the model, which was not fulfilled for large bubbles. Therefore, the energy constraint was underestimated due to the undervaluation of bubble surface area, leading to overpredicted breakup rates of large bubbles in our model[36]. For better prediction of the bubble breakup rate, the bubble shape variations[49] should be considered in detail.
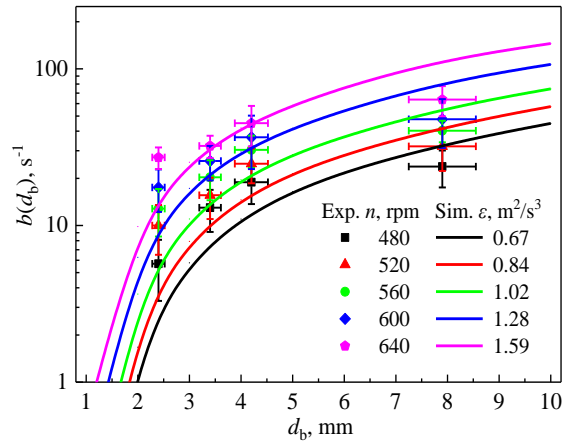
Figure 8. Effect of turbulent dissipation rate on the bubble breakup rate in a water-N_2 system.

3.2.2. Effect of liquid properties

Extensive experiments[12,50-54] showed that liquid viscosity μ_l and surface tension σ_l played a significant role in the bubble breakup. Xing et al.[50] carried out dynamical gas disengagement experiments in a bubble column and found that the effect of increasing μ_l could be divided into two regimes: low viscosity (≤ 8 mPa·s) and high viscosity (> 8 mPa·s). In the low viscosity range, the bubble coalescence was enhanced while the bubble breakup was little affected, and the gas holdup was kept almost unchanged with increasing μ_l. In the high viscosity range, however, the bubble breakup was remarkably

inhibited and the gas holdup decreased significantly. In this work, 54.9% (wt) and 76.6%

(wt) glycerol aqueous solutions were used to study the effect of high μ_l on the bubble

breakup.

Fig. 9 shows the bubble breakup probability and breakup time under different

liquid viscosities. The results showed that with increasing μ_l the bubble breakup

probability slightly decreased in the low viscosity range but significantly decreased in

the high viscosity range. However, the bubble breakup time was only slightly affected,

indicating that the number of effective turbulent eddies with enough collision energy

decreased with increasing liquid viscosity.
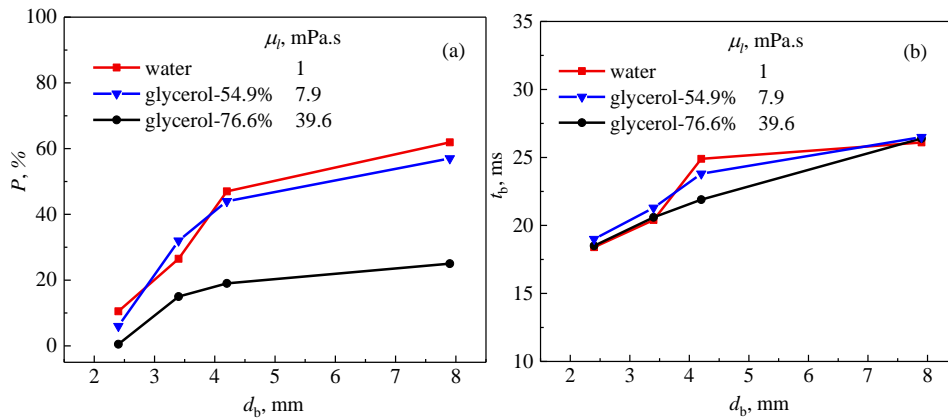
Figure 9. Effect of μ_l on (a) bubble breakup probability and (b) breakup time. (N_2-water

system, $n = 480$ rpm)

As shown in Fig. 10, when $\mu_l \leq 8$ mPa·s, the measured bubble breakup rates and

those predicted by our model[36] were almost independent of μ_l; when $\mu_l > 8$ mPa·s, the

measured and predicted breakup rates significantly decreased with increasing μ_l.

It was reported that decreasing surface tension would significantly increase the

bubble breakup rate.[45,53] Fig. 11 shows the comparison of the bubble breakup rates in

the water-N_2 and ethanol-N_2 systems at an agitation speed of 480 rpm. Both the

experimental and predicted results showed larger bubble breakup rates at lower surface tension. One reason for this trend was that the breakup constraints $\rho_l u_\lambda^2/2 \geq \sigma_l/d_b$, $e(\lambda) \geq \pi d_b^2 \sigma_l(1/f^{1/3}-1)$ were easier to satisfy at a lower surface tension. Another reason was referred to the internal flow mechanism. According to our previous bubble breakup model[36], the internal-flow velocity of the gas flowing from the smaller to larger part of a deformed decreased with decreasing surface tension, which in turn increased the bubble breakup rate.
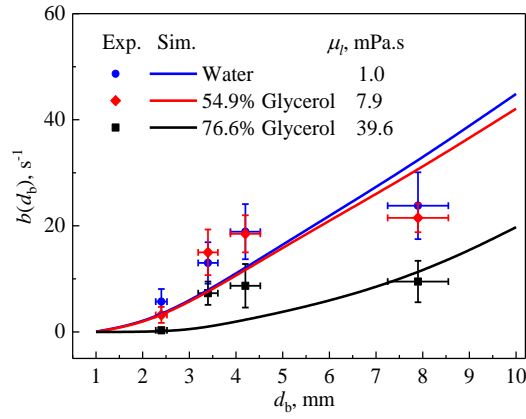
Figure 10. The bubble breakup rates under different liquid viscosities.
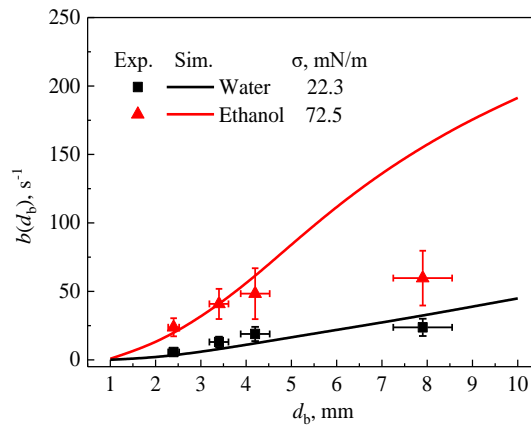
(N_2-water system, $n = 480$ rpm)

Figure 11. The bubble breakup rates under water and ethanol system.

(N_2-water and N_2-ethanol systems, $n = 480$ rpm)

3.2.3. Effect of pressure or gas density

Wilkinson et al.[12] studied the effect of gas density on the bubble breakup by observing the bubble deformation and breakup in a venturi-shaped pipe, and found that the pressure had a significant effect on the bubble breakup. Fig. 12 shows that increasing gas density increased the bubble breakup rate under the water system, which was consistent with the results reported by Wilkinson et al.[12].
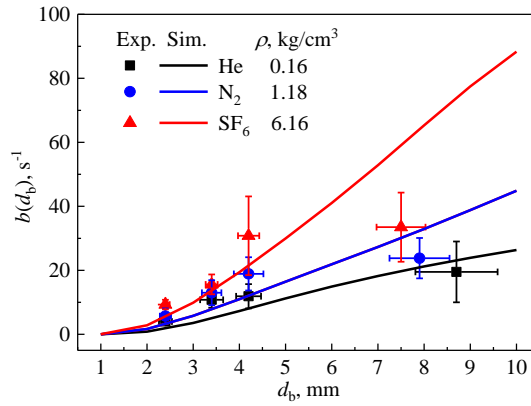

Figure 12. Bubble breakup rates under different pressures or gas densities at n = 480 rpm.

The effect of pressure on the bubble breakup rate at different μ_l is shown in Fig. 13. At low μ_l (water), the bubble breakup rate significantly increased with increasing pressure. In contrast, the effect of pressure on the bubble breakup rate was suppressed at high μ_l (39.6 mPa·s, 76.6% glycerol). The measured bubble breakup rates and those predicted by our breakup model[36] are also compared in Fig. 13, showing consistency in the general trend.
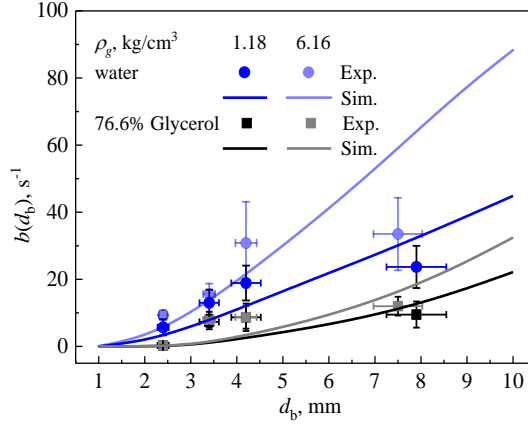
Figure 13. Effect of gas density on bubble breakup rate at different liquid viscosities at $n =$ 480 rpm.

3.2.4. Comparison of bubble breakup rates with the literature

The experimental and predicted dimensionless breakup rates from the literature were collected to compare with our experimental data, as shown in Fig. 14. The dimensionless quantities were defined as:

$$d_b^* = d_b/L \quad \text{and} \quad b(d_b)^* = b(d_b)T \tag{5}$$

where L and T were respectively the length and time scales defined as:

$$L = \left(\frac{\sigma}{\rho_l}\right)^{3/5} \frac{1}{\varepsilon^{2/5}} \tag{6}$$

$$T = \left(\frac{\sigma}{\rho_l}\right)^{2/5} \frac{1}{\varepsilon^{3/5}} \tag{7}$$

From Fig. 14, it could be found that the bubble breakup rates predicted by our improved model[36] were well consistent with both our experimental data and those reported in the literatural[13,19]. However, the breakup model by Luo and Svendsen[47] and our previous model[45] undervalued the bubble breakup rates in the large bubble size range ($d_b^* > 1$), and the model by Zhao and Ge[46] under-predicted the breakup rates in the small bubble size region ($d_b^* \leq 1$). Although the bubble breakup rates predicted by

Razzaghi et al.[48] and Wang et al.[1] were also well consistent with the experimental data, the effect of pressure on the bubble breakup rates could not be predicted by their models. For experimental data, our measured bubble breakup rates were larger than that by Wilkinson et al.[13] in the small bubble size region ($d_b^* \leq 2$), and smaller than that by Martínez-Bazán et al.[19] in the large bubble size region ($d_b^* > 2$).
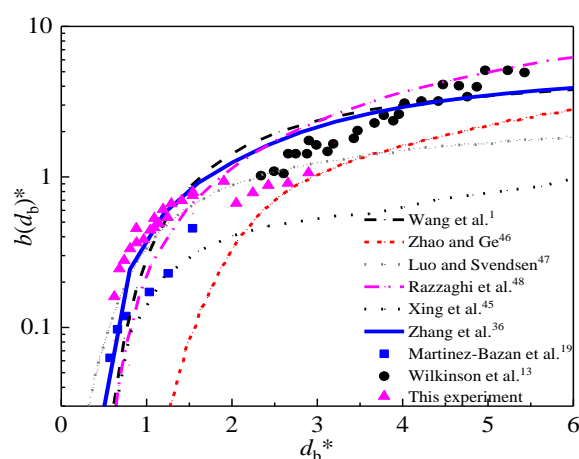

Figure 14. Comparison of experimental data with the predicted and mearsured bubble breakup rates from literature (symbos : experimental, lines : predicted).

3.3. Daughter bubble size distribution

Besides the bubble breakup rate, the daughter bubble size distribution was also needed for solving the PBM equation. In this section, the effect of pressure or gas density, mother bubble size, turbulent dissipation rate and liquid properties on the daughter size distributions were systematically investigated. These experimental data were also important for further validating the bubble breakup model.

Different daughter bubble size distributions have been predicted in the literature, including U-shape[47], Λ-shape[21,55-57], and M-shape[1,46,58,59] daughter size distributions. Many experimental results[14,18,35] showed a U-shape, which might fail to give the true

daughter size distribution because a big interval Δf_v was used. To get a more accurate daughter bubble size distribution, more than 300 cases of bubble breakup were collected in the water-N_2 system using a 4 mm tube. The statistical results showed that daughter bubble size distribution was M-shaped when a small interval of $\Delta f_v = 0.02$ was used, as shown in Fig. 15. In the previous work, Wang et al.[1] have ascribed the results of M-shaped distribution to the equilibrium between two breakup constraints including the pressure constraint and surface energy constraint.
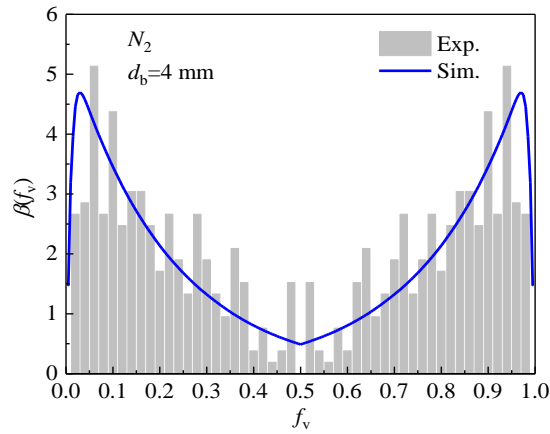

Figure 15. Daughter bubble size distribution in a water-N_2 system at $n = 480$ rpm.

In our experiments, most bubble breakups were binary breakup, and the multiple breakup was actually subsequent binary breakup. As shown in Fig. 16, the mother bubble finally broke up into four daughter bubbles through three binary breakup processes at 21 ms, 30 ms and 36 ms. In this case, the first binary breakup was used to calculate the daughter size distribution.
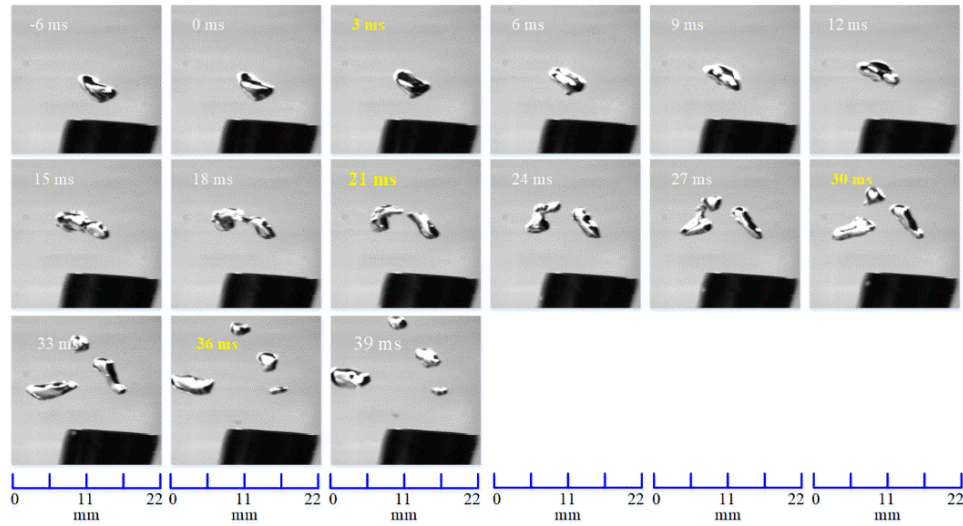
Figure 16. Schematic diagram of continuous binary bubble breakup.

3.3.1. Effect of pressure or gas density

The effect of pressure or gas density on the daughter bubble size distribution is shown in Fig. 17. The probability of equal-size breakup increased with increasing gas density, which was consistent with the model predictions[36] and could be explained by the internal flow mechanism[12,32,35]. According to our previous model[36], the internal-flow velocity for gas flowing from the smaller to the larger part of a deformed bubble decreased with increasing gas density, thus increased the probability of equal-size breakup. To validate this mechanism, two bubbles with different gas densities (N_2 and SF_6) were released simultaneously to study their breakup behaviors. One typical comparison is shown in Fig. 18. In the same period, the gas in the smaller part of the SF_6 bubble hardly flowed into the larger part and an equal-size breakup happened. However, a long bubble neck was formed and the gas flowed fastly into the larger part in the N_2 bubble. For statistic, the experiemtns were repeated for 40 times and 90% of the results showed that the internal flow was faster in lower gas density.
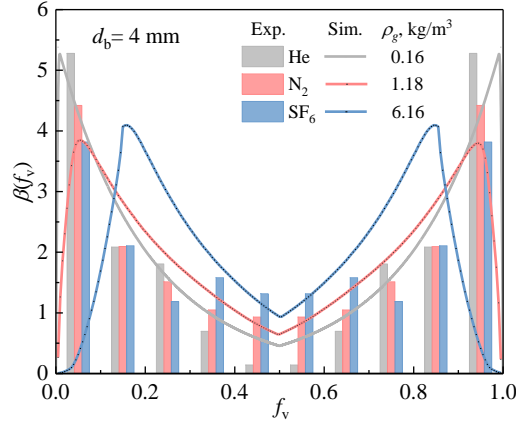
Figure 17. Effect of pressure or gas density on daughter bubble size distributions; water system, $n = 480$ rpm, $d_b = 4$ mm, $\Delta f_v = 0.1$.
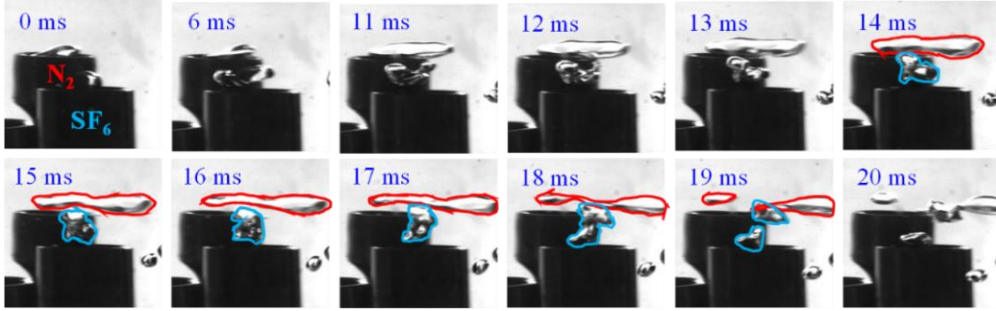

Figure 18. Deformation and breakup of the bubbles with different gas densities. (N_2/SF_6 and water system, $d_b = 4$ mm)

3.3.2. Effect of turbulent dissipation rate

Figure 19 shows the effect of agitation speed on the daughter bubble size distribution. The experimental results showed that a higher probability of equal-size breakup was obtained at a higher agitation speed due to the increased turbulent eddy velocity. According to the internal flow mechanism[36], with increasing turbulent dissipation rate, the time for the shrinking of bubble neck decreased, which decreased the volume of gas flowing from the smaller to larger part. Note that the increase in the probability of equal-size breakup under high turbulent dissipation rates was under-predicted by our model[36].
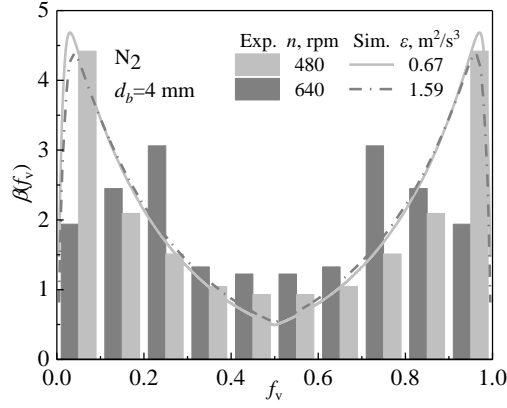
Figure 19. Effect of agitation speed on daughter bubble size distributions.

(N_2-water, d_b = 4 mm, Δf_v = 0.1)

3.3.3. Effect of surface tension

The effect of σ_l on the daughter size distribution is shown in Fig. 20. Both the experimental and predicted results showed that the probability of equal-size breakup increased with decreasing σ_l. At a low σ_l, the driving force for the internal flow decreased, thus the internal-flow velocity was smaller and the probability of equal-size breakup was increased.

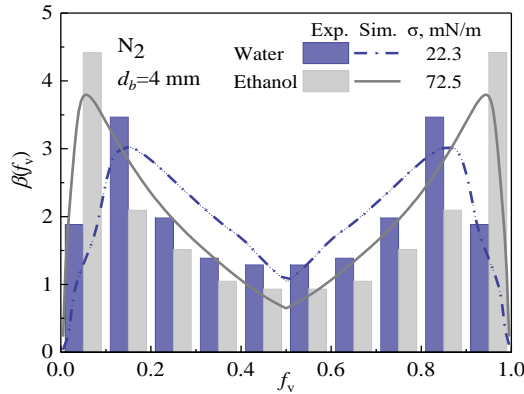

Figure 20. Effect of σ_l on daughter bubble size distributions.

(N_2-water/ethanol system, n = 480 rpm, d_b = 4 mm, Δf_v = 0.1)

3.3.4. Effect of mother bubble diameter

The bubble breakup models of Luo and Svendsen[47] and Zhao and Ge[46] predicted

that the increasing d_b increased the probability of equal-size breakup, while the models of Wang et al.[1], Martínez-Bazán et al.[19], Lehr et al.[2] and Razzaghi et al.[48] predicted an opposite trend. Herein the effect of d_b on the daughter size distribution was studied with Helium bubbles of 4.2 mm and 8.6 mm. As shown in Fig. 21, a higher probability of equal-size breakup was obtained with the larger d_b. Without considering the internal flow, the larger d_b would contribute to a higher increase in surface energy $e(\lambda) \geq \pi d_b^2 \sigma (1/f^{1/3}-1)$, leading to lower probability of equal-size breakup. However, with considering the internal flow, according to the internal flow mechanism[36], the Laplace pressure decreased with increasing d_b, leading to a smaller velocity of internal flow and decreased ability to redistribute the mother bubble. As a result, the probability of equal-size breakup increased with an increase in d_b. Therefore, the effect of d_b on daughter size distribution predicted by our internal-flow breakup model[36] was in a good agreement with the experimental trend. Furthermore, the predicted daughter size distributions were consistent with the experimental data.
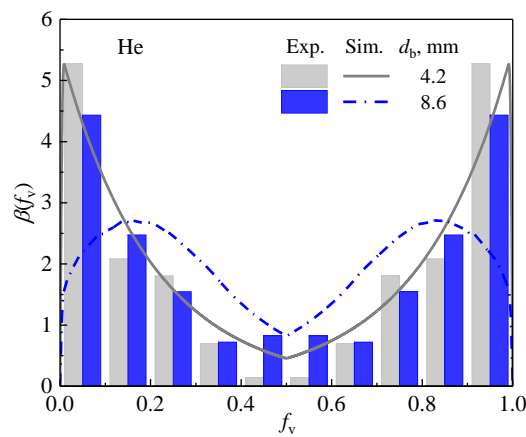

Figure 21. The effect of d_b on daughter bubble size distributions; He-water, n = 480 rpm, Δf_v = 0.1.

4. Conclsuions

The bubble breakup behaviors in a specially designed stirred tank for producing relatively homogeneous turbulent flow were studied by a high-speed camera. An M-shaped daughter size distribution was observed. The effects of the agitation speed, mother bubble size, liquid properties and gas density on the bubble breakup were systematically investigated. Higher agitation speed, gas density or pressure, larger mother bubble size and lower surface tension increased the breakup rates and probability of equal-size breakup. The bubble breakup rates were independent on liquid viscosity at $\mu_l \leq 8$ mPa·s, but significantly decreased with increasing μ_l at $\mu_l > 8$ mPa·s. In addition, the internal flow mechanism was clearly observed and illustrated, which accounted for the effect of gas density or operating pressure on the bubble breakup. With the internal-flow mechanism, our previous breakup model could well predict the effect of gas density, turbulent dissipation rate, surface tension and mother bubble size on the bubble breakup rate and daughter bubble size distribution.

Acknowledgments

Notation

$b(d_b)$, $b(v)$ bubble breakup rate, s^{-1}

$c(v,v')$ bubble coalescence rate, s^{-1}

d_t the diameter of tube, mm

d_b the diameter of mother bubble, mm

$e(\lambda)$	turbulent energy of an eddy with size λ, J
f_v	bubble breakup ratio, dimensionless
Δf_v	interval of breakup ration, dimensionless
n	agitation speed, rpm
$n(v, t)$	number density of bubble, m^{-3}
$P(d_b)$	bubble breakup probability, %
r	the radial coordinate, m
t_b	bubble breakup time, ms
t_1	time scale for internal flow, s
u_λ	turbulent eddy velocity, m·s^{-1}
U_{neck}	internal gas flow velocity, m·s^{-1}
U_θ	Mean tangential velocity, cm·s^{-1}
U_r	Mean radial velocity, cm·s^{-1}
U_z	Mean axial velocity, cm·s^{-1}
z	the axial coordinate, m

Greek letters

ρ_g	gas density, kg·m^{-3}
ρ_l	liquid density, kg·m^{-3}
σ_l	liquid surface tension, mN·m^{-1}
μ_l	liquid viscosity, mPa·s
ε	turbulent dissipation rate, m^2·s^{-3}
$\beta(v,v'), \beta(f_v)$	bubble size distribution, dimensionless

σ_d standard deviation of mother bubble, $\sigma_d = \sqrt{\sum_{i=1}^{N}(d_i - d_\mathrm{b})^2 / N}$, mm

σ_b standard deviation of bubble breakup rate, $\sigma_b = \sqrt{\sum_{i=1}^{N}(b_{d_i} - b_{d_\mathrm{b}})^2 / N}$, s^{-1}

γ breakup probability function, dimensionless

References

1. Wang TF, Wang JF, Jin Y. A novel theoretical breakup kernel function for bubbles/droplets in a turbulent flow. *Chem Eng Sci.* 2003;58(20):4629-4637.

2. Lehr F, Millies M, Mewes D. Bubble-size distributions and flow fields in bubble columns. *AIChE J.* 2002;48(11):2426-2443.

3. Wang TF, Wang JF. Numerical simulations of gas–liquid mass transfer in bubble columns with a CFD–PBM coupled model. *Chem Eng Sci.* 2007;62(24):7107-7118.

4. Zhang HH, Guo KY, Wang YL, Sayyar A, Wang TF. Numerical simulations of the effect of liquid viscosity on gas-liquid mass transfer of a bubble column with a CFD-PBM coupled model. *Int J Heat Mass Tran.* 2020;161:120229.

5. Zhang HH, Sayyar A, Wang YL, Wang TF. Generality of the CFD-PBM coupled model for bubble column simulation. *Chem Eng Sci.* 2020;219:115514.

6. Shu SL, Vidal D, Bertrand F, Chaouki J. Multiscale multiphase phenomena in bubble column reactors: A review. *Renew Energ.* 2019;141:613-631.

7. Hulburt HM, Katz S. Some problems in particle technology: A statistical mechanical formulation. *Chem Eng Sci.* 1964;19(8):555-574.

8. Wang TF, Wang JF, Jin Y. A CFD-PBM coupled model for gas-liquid flows. *AIChE J.* 2006;52(1):125-140.

9. Ramkrishna D, Mahoney AW. Population balance modeling. Promise for the future. *Chem Eng Sci.* 2002;57(4):595-606.

10. Liao YX, Lucas D. A literature review of theoretical models for drop and bubble breakup in turbulent dispersions. *Chem Eng Sci.* 2009;64(15):3389-3406.

11. Solsvik J, Tangen S, Jakobsen HA. On the constitutive equations for fluid particle breakage. *Rev Chem Eng.* 2013;29(5):241-356.

12. Wilkinson PM, Vanschayk A, Spronken JPM, Vandierendonck LL. The influence of

gas-density and liquid properties on bubble breakup. *Chem Eng Sci.* 1993;48(7):1213-1226.

13. Wilkinson PM, Vondierendonck LL. Pressure and gas-density effects on bubble break-up and gas hold-up in bubble-columns. *Chem Eng Sci*. 1990;45(8):2309-2315.

14. Hesketh RP, Etchells AW, Russell TWF. Experimental-observations of bubble breakage in turbulent-flow. *Ind Eng Chem Res*. 1991;30(5):835-841.

15. Vankova N, Tcholakova S, Denkov ND, Vulchev VD, Danner T. Emulsification in turbulent flow: 2. Breakage rate constants. *J Colloid Interf Sci*. 2007;313(2):612-629.

16. Tcholakova S, Vankova N, Denkov ND, Danner T. Emulsification in turbulent flow: 3. Daughter drop-size distribution. *J Colloid Interf Sci*. 2007;310(2):570-589.

17. Vankova N, Tcholakova S, Denkov ND, Ivanov IB, Vulchev VD, Danner T. Emulsification in turbulent flow: 1. Mean and maximum drop diameters in inertial and viscous regimes. *J Colloid Interf Sci*. 2007;312(2):363-380.

18. Vejražka J, Zedníková M, Stanovský P. Experiments on breakup of bubbles in a turbulent flow. *AIChE J*. 2018;64(2):740-757.

19. Martínez-Bazán C, Montañés JL, Lasheras JC. On the breakup of an air bubble injected into a fully developed turbulent flow. Part 1. Breakup frequency. *J Fluid Mech*. 1999;401:157-182.

20. Martínez-Bazán C, Montañés JL, Lasheras JC. Bubble size distribution resulting from the breakup of an air cavity injected into a turbulent water jet. *Phys Fluids*. 1999;12(1):145-148.

21. Martínez-Bazán C, Montañés JL, Lasheras JC. On the breakup of an air bubble injected into a fully developed turbulent flow. Part 2. Size PDF of the resulting daughter bubbles. *J Fluid Mech*. 1999;401:183-207.

22. Eastwood CD, Armi L, Lasheras JC. The breakup of immiscible fluids in turbulent flows. *J Fluid Mech*. 2004;502:309-333.

23. Risso F, Fabre J. Oscillations and breakup of a bubble immersed in a turbulent field. *J Fluid Mech*. 1998;372:323-355.

24. Maaß S, Kraume M. Determination of breakage rates using single drop experiments.

Chem Eng Sci. 2012;70:146-164.

25. Hasan BO. Experimental study on the bubble breakage in a stirred tank Part 2: Local dependence of breakage events. *Exp Therm Fluid Sci*. 2018;96:48-62.

26. Solsvik J, Jakobsen HA. Single drop breakup experiments in stirred liquid-liquid tank. *Chem Eng Sci*. 2015;131:219-234.

27. Maaß S, Gäbler A, Zaccone A, Paschedag AR, Kraume M. Experimental investigations and modelling of breakage phenomena in stirred liquid/liquid systems. *Chem Eng Res Des*. 2007;85(5):703-709.

28. Maaß S, Buscher S, Hermann S, Kraume M. Analysis of particle strain in stirred bioreactors by drop breakage investigations. *Biotechnol J*. 2011;6(8):979-992.

29. Maaß S, Metz F, Rehm T, Kraume M. Prediction of drop sizes for liquid–liquid systems in stirred slim reactors—Part I: Single stage impellers. *Chem Eng J*. 2010;162(2):792-801.

30. Hasan BO. Experimental study on the bubble breakage in a stirred tank. Part 1. Mechanism and effect of operating parameters. *Int J Multiphas Flow*. 2017;97:94-108.

31. Zhou H, Yu X, Jing S, Zhou H, Lan W, Li S. Measurement of droplet breakage in a pump-mixer. *Chem Eng Sci*. 2019;195:23-38.

32. Ravelet F, Colin C, Risso F. On the dynamics and breakup of a bubble rising in a turbulent flow. *Phys Fluids*. 2011;23(10).

33. Wichterle K, Wichterlova J, Kulhankova L. Breakup of bubbles rising in liquids of low and moderate viscosity. *Chem Eng Commun*. 2005;192(5):550-556.

34. Andersson R, Andersson B. Modeling the breakup of fluid particles in turbulent flows. *AIChE J*. 2006;52(6):2031-2038.

35. Andersson R, Andersson B. On the breakup of fluid particles in turbulent flows. *AIChE J*. 2006;52(6):2020-2030.

36. Zhang HH, Yang GY, Sayyar A, Wang TF. An improved bubble breakup model in turbulent flow. *Chem Eng J*. 2020;386:121484.

37. Coulaloglou CA, Tavlarides LL. Description of interaction processes in agitated liquid-liquid dispersions. *Chem Eng Sci*. 1977;32(11):1289-1297.

38. Montante G, Paglianti A, Magelli F. Experimental analysis and computational

modelling of gas–liquid stirred vessels. *Chem Eng Res Des*. 2007;85(5):647-653.

39. Shi P, Rzehak R. Bubbly flow in stirred tanks: Euler-Euler/RANS modeling. *Chem Eng Sci*. 2018;190:419-435.

40. Basavarajappa M, Draper T, Toth P, Ring TA, Miskovic S. Numerical and experimental investigation of single phase flow characteristics in stirred tanks using Rushton turbine and flotation impeller. *Miner Eng*. 2015;83:156-167.

41. Aubin J, Fletcher DF, Xuereb C. Modeling turbulent flow in stirred tanks with CFD: the influence of the modeling approach, turbulence model and numerical scheme. *Exp Therm Fluid Sci*. 2004;28(5):431-445.

42. Sahu AK, Kumar P, Patwardhan AW, Joshi JB. CFD modelling and mixing in stirred tanks. *Chem Eng Sci*. 1999;54(13):2285-2293.

43. Wu H, Patterson GK. Laser-Doppler measurements of turbulent-flow parameters in a stirred mixer. *Chem Eng Sci*. 1989;44(10):2207-2221.

44. Solsvik J, Jakobsen HA. Single Air bubble breakup experiments in stirred water tank. *Int J Chem React Eng*. 2015;13(4):477-491.

45. Xing CT, Wang TF, Guo KY, Wang JF. A unified theoretical model for breakup of bubbles and droplets in turbulent flows. *AIChE J*. 2015;61(4):1391-1403.

46. Zhao H, Ge W. A theoretical bubble breakup model for slurry beds or three-phase fluidized beds under high pressure. *Chem Eng Sci*. 2007;62(1-2):109-115.

47. Luo H, Svendsen HF. Theoretical model for drop and bubble breakup in turbulent dispersions. *AIChE J*. 1996;42(5):1225-1233.

48. Razzaghi K, Shahraki F. Theoretical model for multiple breakup of fluid particles in turbulent flow field. *AIChE J*. 2016;62(12):4508-4525.

49. Shi WB, Yang J, Li G, Yang XG, Zong Y, Cai XY. Modelling of breakage rate and bubble size distribution in bubble columns accounting for bubble shape variations. *Chem Eng Sci*. 2018;187:391-405.

50. Xing CT, Wang TF, Wang JF. Experimental study and numerical simulation with a coupled CFD–PBM model of the effect of liquid viscosity in a bubble column. *Chem Eng Sci*. 2013;95:313-322.

51. Guo KY, Wang TF, Liu YF, Wang JF. CFD-PBM simulations of a bubble column

with different liquid properties. *Chem Eng J*. 2017;329:116-127.

52. Chaumat H, Billet AM, Delmas H. Hydrodynamics and mass transfer in bubble column: Influence of liquid phase surface tension. *Chem Eng Sci*. 2007;62(24):7378-7390.

53. Götz M, Lefebvre J, Mörs F, Reimert R, Graf F, Kolb T. Hydrodynamics of organic and ionic liquids in a slurry bubble column reactor operated at elevated temperatures. *Chem Eng J*. 2016;286:348-360.

54. Götz M, Lefebvre J, Mörs F, et al. Novel gas holdup correlation for slurry bubble column reactors operated in the homogeneous regime. *Chem Eng J*. 2017;308:1209-1224.

55. Han LC, Gong SG, Ding YW, Fu J, Gao NN, Luo HA. Consideration of low viscous droplet breakage in the framework of the wide energy spectrum and the multiple fragments. *AIChE J*. 2015;61(7):2147-2168.

56. Han LC, Gong SG, Li YQ, Ai QH, Luo HA, Liu ZF. A novel theoretical model of breakage rate and daughter size distribution for droplet in turbulent flows. *Chem Eng Sci*. 2013;102:186-199.

57. Han LC, Luo HA, Liu YJ. A theoretical model for droplet breakup in turbulent dispersions. *Chem Eng Sci*. 2011;66(4):766-776.

58. Lehr F, Mewes D. A transport equation for the interfacial area density applied to bubble columns. *Chem Eng Sci*. 2001;56(3):1159-1166.

59. Prince MJ, Blanch HW. Bubble coalescence and break-up in air-sparged bubble columns. *AIChE J*. 1990;36(10):1485-1499.

Supporting Information

Validation of the RANS k-ε model

The accuracy and reliability of the Reynolds-averaged Navier-Stokes (RANS) two-fluid model and *k-ε* turbulence model were validated by simulating the same stirred tank reported by Wu and Patterson[1] and comparing with their experimnetal data. Figs. S1-S3 show the comparison of the simulated mean tangential velocity, radial velocity and axial velocity profiles with the experimental results at different radial positions. A good agreement was obtained between the simulated and experimental results, which validated the accuracy and reliability of the RANS *k-ε* model for simulating the stirred tank.
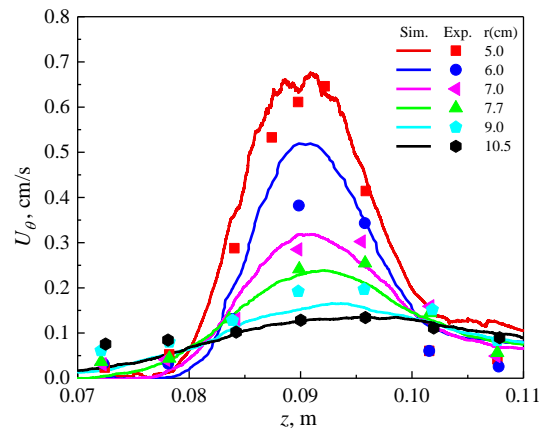

Figure S1. Mean tangential velocity profiles at various radial positions.
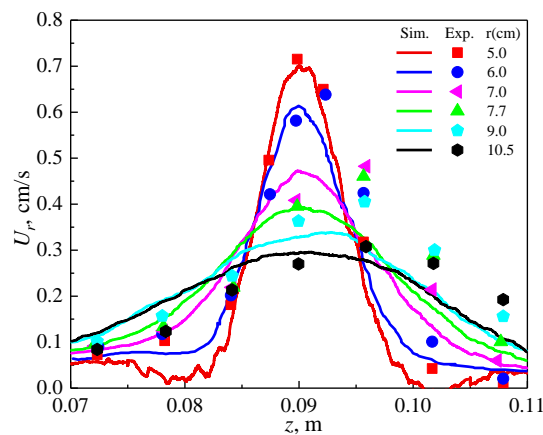

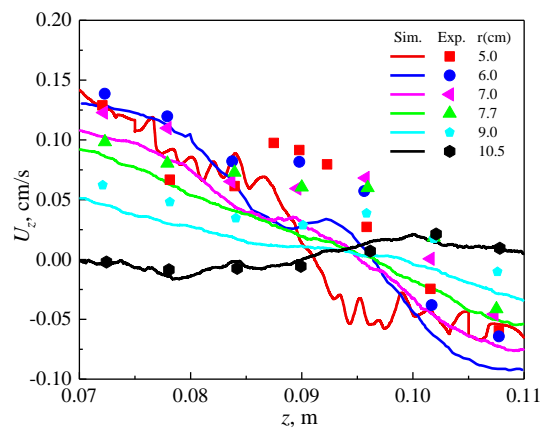Figure S2. Mean radial velocity profiles at various radial positions.

Figure S3. Mean axial velocity profiles at various radial positions.

[1] Wu H, Patterson GK. Laser-Doppler measurements of turbulent-flow parameters in a stirred mixer. *Chem Eng Sci*. 1989;44(10):2207-2221.